# Computational Design of an Intramolecular Frustrated Lewis Pair Catalyst for Enantioselective Hydrogenation

Gitanjali Sharma, Paul D. Newman, Rebecca Melen, James A. Platts*
School of Chemistry, Cardiff University, Park Place, Cardiff CF10 3AT, UK.

* Author for correspondence: Tel +44-2920-874950, Email: platts@cardiff.ac.uk

**Abstract**

We report DFT calculations on potential intramolecular, enantioselective hydrogenation catalysts based around borenium-carbenes based on a camphor scaffold. Using the M06-2X meta-hybrid functional, we find frustrated Lewis pair (FLP) behaviour with suitably chosen linkers that prevent association of Lewis bases with the borenium centre. These intramolecular FLPs are predicted to be able to heterolytically dissociate $H_2$. Barriers to dissociation and the and endo/exo-ergic nature of the reaction can be tuned by the nature of the base and substituent on B. The reactivity of the hydrogenated FLP catalyst with olefin and carbonyl substrates is then explored: we predict concerted reactions for all substrates considered with relatively low barriers and large exoergic character. Hydrogenation of both faces of a prochiral substrate is also examined, indicating a small but significant variation in reaction barrier in favour of the *Si*-face, ascribed to stronger interactions with the aromatic $\pi$-system in the TS compared to the *Re*-face.

**Introduction**

Frustrated Lewis Pair (FLP) chemistry and its use in metal-free catalysis is an area of great current interest.[1] The inability of sterically overcrowded Lewis pairs to form classical adducts has been known since 1942,[2] but it was in 2006 that unconventional reactivity of such adducts was uncovered by Stephan and his group,[3] who coined the term FLP, reporting that intra- as well as inter-molecular FLPs that were able to split dihydrogen. Since then there has been rapid proliferation, as described in numerous excellent reviews.[4] Application to a wide range of catalytic reactions and a variety of substrates has been demonstrated, with particular focus on hydrogenation.[5] The ability of FLPs to split hydrogen and then release to a chosen substrate is well documented,[6] although other sources of hydrogen have also been explored. Computational modelling has played an increasing role in design of novel FLP catalysts, with density functional theory (DFT) to the fore.[7]

Many FLP systems reported are intermolecular in nature, consisting of strong Lewis acids and bases that are prevented from close approach by steric effects. Our laboratory has an interest in design in intramolecular FLPs, in which pre-organisation effects might facilitate new or improved reactivity profiles. Suitable design of such a FLP might also allow for design of enantioselective hydrogenation catalysts by incorporating chiral elements in the catalytic site. To that end, we have been working towards synthesis of a FLP incorporating a chiral carbene based on a camphor backbone coupled to a borenium Lewis acid centre.[8] A modular design allows different Lewis bases and substituents on boron, with the goal of tuning reactivity. Scheme 1 sets out the general design principles, where X, Y and Z can be varied, with Y containing a Lewis base that with suitable design cannot form an associated Lewis pair with the Lewis acidic borenium centre.

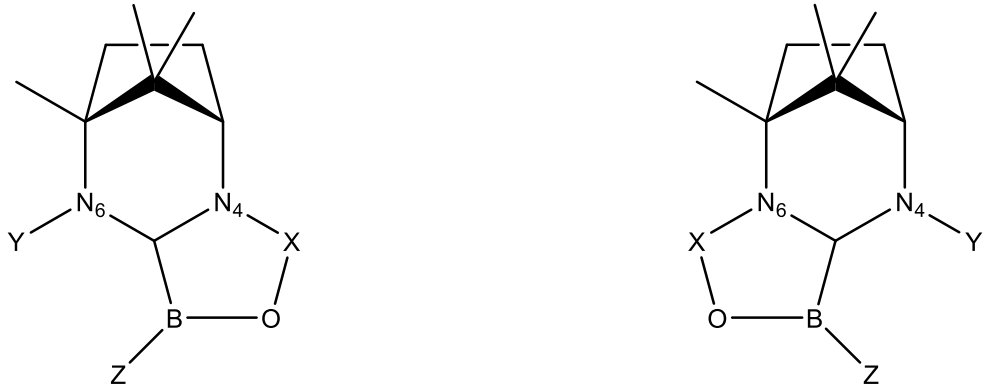


**1** **2**

**Scheme 1**: Structure and numbering of potential catalysts **1** and **2**

In order to guide synthetic strategies, we report here DFT calculations on the structure, properties and reactivity of a range of molecules based on these general scaffolds. DFT has been widely used to examine and predict FLP behaviour, including structural studies of FLPs[9] as well as mechanistic descriptions of hydrogenation,[10] $CO_2$ activation,[11] borylation,[12] and hydroboration.[13] Here, we have used a combination of potential energy surfaces with properties derived from electron density and natural bonding orbitals (NBO) to determine those choices of X, Y and Z that are predicted to give rise to desirable characteristics for an enantioselective hydrogenation catalyst.

**Computational Methods**

All DFT optimisations employed the M06-2X meta-hybrid functional[14], typically with the 6-31G(d)[15] basis set within the Gaussian09 package.[16] We note that M06-2X has been widely used in theoretical studies of FLP chemistry, though its suitability for the systems under study here has been checked against experiment (*vide infra*). All species were fully geometry optimised without constraint, and confirmed as minima or transition states *via* harmonic frequency calculation with the same method and basis set. Thermochemical data at 298 K was extracted from these calculations. Intrinsic reaction coordinate (IRC) confirmed that transition states located properly link the expected reactants and products. Single point energy calculations at stationary points were performed at 6-311+G(d,p) level within a polarized continuum model (PCM) simulation of toluene solvent,[17] Natural bond order (NBO)

analysis[18] was performed in G09, QTAIM analysis[19] employed AIMAll,[20] and NCI images were obtained using NCIPlot.[21]

## Results and Discussion

*i) Methodology*

In order to test the suitability of theoretical methods for description of carbene-borenium FLP systems, selected geometrical parameters were compared against X-ray crystallographic values for two molecules, **3** and **4**, as reported in Table 1. B—C bond lengths vary somewhat dependent on functional, whereas C—N lengths are less variable. The data presented also shows that basis set dependence of key bond lengths is small, such that the relatively small and quick 6-31G(d) basis is used for all geometry optimisation and vibrational frequency calculations. Overall, the M06-2X functional provides excellent agreement with experiment, so unless otherwise stated this method is used throughout.

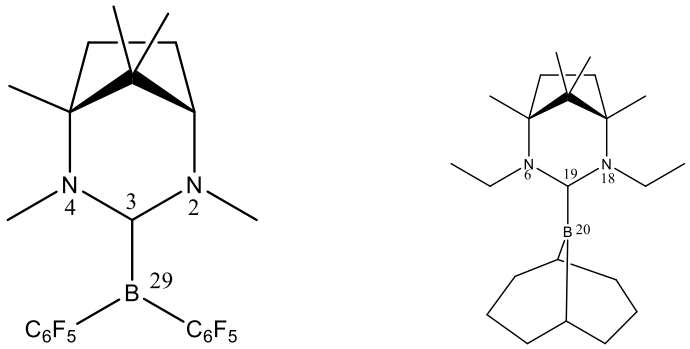


**Scheme 2**: Structure and numbering of molecules **3** and **4**

**Table 1**: Comparison of DFT with experimental bond lengths for molecules **3** and **4** (Å)

| | **Bond** | **Length** | **Bond** | **Length** | **Bond** | **Length** |
|---|---|---|---|---|---|---|
| **3** | | | | | | |
| Experimental | C3-B29 | 1.637 | C3-N4 | 1.347 | C3-N2 | 1.323 |
| B3LYP/6-31G(d) | | 1.655 | | 1.351 | | 1.341 |
| PBE/6-31G(d) | | 1.645 | | 1.358 | | 1.348 |
| PBE0/6-31G(d) | | 1.643 | | 1.344 | | 1.334 |
| B97D/6-31G(d) | | 1.656 | | 1.355 | | 1.344 |
| WB97xD/6-31G(d) | | 1.646 | | 1.344 | | 1.333 |
| M062X/6-31G(d) | | 1.647 | | 1.343 | | 1.332 |
| M062X/6-311G(d) | | 1.645 | | 1.341 | | 1.330 |
| M062X/6-311+G(d,p) | | 1.646 | | 1.341 | | 1.330 |
| **4** | | | | | | |
| Experimental | C19-B20 | 1.693 | C19-N6 | 1.371 | C19-N18 | 1.351 |
| B3LYP/6-31G(d) | | 1.673 | | 1.363 | | 1.358 |
| PBE/6-31G(d) | | 1.663 | | 1.350 | | 1.366 |
| PBE0/6-31G(d) | | 1.664 | | 1.354 | | 1.341 |
| B97D/6-31G(d) | | 1.671 | | 1.358 | | 1.364 |
| WB97xD/6-31G(d) | | 1.666 | | 1.352 | | 1.320 |
| M062X/6-31G(d) | | 1.672 | | 1.362 | | 1.349 |
| M062X/6-311G(d) | | 1.671 | | 1.361 | | 1.347 |
| M062X/6-311+G(d,p) | | 1.671 | | 1.361 | | 1.348 |

*ii) Structure*

Using this method, two categories of structure, **1** and **2** (Scheme 1) were chosen as possible scaffolds for intramolecular FLP-based chiral hydrogenation catalysts. The relative molar energy of molecules with different linker (X), holding substituents Y and Z fixed as $CH_3$ for now, after optimization is reported in Table 2. Energetic preference for the position of the linker varies with its nature: shorter alkyl chains are preferred on the methyl side, whereas

longer chains and aromatic linkers prefer the non-methyl side. We ascribe this to a change between FLP and conventional Lewis pair behaviour on extension of the linker (*vide infra*). Between isomeric linkers $CH_2C_6H_4O$ and $C_6H_4CH_2O$, the former is preferred by a significant amount.

**Table 2** Relative molar energies [a] of variations on **1** and **2** after optimization (kJ $mol^{-1}$): Y and Z fixed at $CH_3$

| | **X** | **1** | **2** |
|---|---|---|---|
| a | $CH_2$ | +6.89 | 0.00 |
| b | $CH_2CH_2$ | +1.16 | 0.00 |
| c | $CH_2CH_2CH_2$ | 0.00 | +3.32 |
| d | $C_6H_4$ | 0.00 | +32.40 |
| e | $CH_2C_6H_4O$ | +0.21 | 0.00 |
| f | $C_6H_4CH_2O$ | 0.00 | +13.79 |

[a] Defined as energy difference between isomers **1** and **2**, expressed as a molar quantity, taking the more stable as zero

After screening for stable linkers, Hydrogen Ion Affinity (HIA) and Fluoride Ion Affinity (FIA) was calculated to determine the Lewis acid strength of the borenium centre (Table 3). These calculations used BP86/SVP, as this is reported to yield better comparisons to the experimental values.[22] This data indicates that these systems are markedly stronger Lewis acids compared to neutral reference acids (HIA for $BF_3$ = 297, $BCl_3$ = 395, $BBr_3$ = 440 kJ $mol^{-1}$), due to the formal positive charge on the borenium centre.

**Table 3** HIA and FIA values for the stable linkers carried out at BP86/SVP level (kJ/mol).

| Compound | HIA | FIA |
|---|---|---|
| **2a** (X=$CH_2$) | 652.4 | 647.0 |
| **2b** (X=$CH_2CH_2$) | 641.1 | 634.9 |
| **1c** (X=$CH_2CH_2CH_2$) | 619.3 | 607.9 |
| **1d** (X=$C_6H_4$) | 666.1 | 656.2 |
| **2e** (X= $CH_2C_6H_4O$) | 632.7 | 624.6 |

Intramolecular FLPs were constructed, initially from **2a** (*i.e.* with X = $CH_2$ and Z = $CH_3$) and a range of bases Y. Molecules with Y = $CH_2X$, where X is an amine, phosphine or hydroxyl form FLP, as judged by a bond order close to zero. Aniline bases, with N in any of *ortho*-, *meta*- or *para*- position also result in FLP behaviour. In contrast, Y = $CH_2CH_2X$ forms conventional Lewis pairs, with bond order of 0.5 or more.

**Table 3** Wiberg B…N bond orders for potential FLPs based on **2a**

| **Y** | **B…N Bond order** |
|---|---|
| $CH_2NH_2$ | 0.001 |
| $CH_2NMe_2$ | 0.002 |
| $CH_2PH_2$ | 0.002 |
| $CH_2PMe_2$ | 0.002 |
| $CH_2OH$ | 0.003 |
| $CH_2CH_2NH_2$ | 0.580 |
| $CH_2CH_2NMe_2$ | 0.530 |
| $CH_2CH_2PMe_2$ | 0.888 |
| $CH_2CH_2OH$ | 0.439 |
| $C_6H_4$-p-$NH_2$ | 0.000 |
| $C_6H_4$-m-$NH_2$ | 0.000 |
| $C_6H_4$-o-$NH_2$ | 0.000 |
| $CH_2$-2pyridine | 0.000 |
| $CH_2$-furan | 0.000 |
| $CH_2$-thiophene | 0.000 |

*iii) Hydrogen dissociation*

For species based on **2a** that exhibited FLP behaviour, DFT was used to probe their ability to heterolytically dissociate $H_2$. This was achieved first by means of relaxed potential energy scan, linking reaction end points consisting of 1) an intermolecular complex of $H_2$ with FLP,

and 2) heterolytic dissociation of $H_2$ with protonated base and hydride attached to boron. Transition state searching from the maximum of the relaxed PES yielded a stationary point with exactly one imaginary frequency, the normal mode of which corresponded with H—H stretching: the correct identity of the TS located was confirmed by use of intrinsic reaction coordinate. Free energies resulting from these calculations with different bases are shown in Table 4: dissociation was observed in most cases, except for when the base was furan or thiophene, which are apparently too weak to dissociate $H_2$. Results corrected for the effect of toluene solvent are also reported in Table 4b, which show the same general trend but with changes in relative energies of up to 20 kJ $mol^{-1}$.

**Table 4a** Free energy profile for $H_2$ dissociation in gas phase (kJ $mol^{-1}$)

| **X** | **Y** | **Z** | **$\Delta G^{‡}$** | **$\Delta G$** |
|---|---|---|---|---|
| $CH_2$ | $CH_2NH_2$ | $CH_3$ | 91.19 | +84.25 |
| $CH_2$ | $CH_2NH_2$ | $C_6F_5$ | 67.84 | +32.68 |
| $CH_2$ | $CH_2NMe_2$ | $CH_3$ | 80.09 | +51.23 |
| $CH_2$ | $CH_2NMe_2$ | $C_6F_5$ | 85.74 | +36.81 |
| $CH_2$ | $CH_2PH_2$ | $CH_3$ | 184.2 | +169.2 |
| $CH_2$ | $CH_2PH_2$ | $C_6F_5$ | 112.58 | +100.73 |
| $CH_2$ | $CH_2PMe_2$ | $CH_3$ | 116.12 | +102.26 |
| $CH_2$ | $CH_2PMe_2$ | $C_6F_5$ | 37.74 | -15.19 |
| $CH_2$ | $CH_2$-2pyridine | $CH_3$ | 127.91 | +84.13 |
| $CH_2$ | $CH_2$-2pyridine | $C_6F_5$ | 143.49 | +102.33 |
| $CH_2$ | $CH_2$-furan | $CH_3$ | - | - |
| $CH_2$ | $CH_2$-thiophene | $CH_3$ | - | - |

**Table 4b** Free energy profile for $H_2$ dissociation in toluene (kJ $mol^{-1}$)

| X | Y | Z | $\Delta G^{‡}$ | ΔG |
|---|---|---|---|---|
| $CH_2$ | $CH_2NH_2$ | $CH_3$ | 80.54 | +51.03 |
| $CH_2$ | $CH_2NH_2$ | $C_6F_5$ | 63.33 | +8.7 |
| $CH_2$ | $CH_2NMe_2$ | $CH_3$ | 60.42 | +12.67 |
| $CH_2$ | $CH_2NMe_2$ | $C_6F_5$ | 78.00 | +6.28 |
| $CH_2$ | $CH_2PH_2$ | $CH_3$ | 184.39 | +151.78 |
| $CH_2$ | $CH_2PH_2$ | $C_6F_5$ | 110.47 | +81.65 |
| $CH_2$ | $CH_2PMe_2$ | $CH_3$ | 117.61 | +69.52 |
| $CH_2$ | $CH_2PMe_2$ | $C_6F_5$ | 35.01 | -43.45 |
| $CH_2$ | $CH_2$-2pyridine | $CH_3$ | 127.91 | +84.13 |
| $CH_2$ | $CH_2$-2pyridine | $C_6F_5$ | 143.49 | +102.33 |

In general, we find a substantial barrier to dissociation of $H_2$, albeit with a wide range from relatively small (35 kJ $mol^{-1}$ for tertiary phosphine with $C_6F_5$ substituent on B) to very high (184 kJ $mol^{-1}$ for primary phosphine with $CH_3$ substituent). In most but not all cases, the electron withdrawing $C_6F_5$ group reduces the barrier. Almost all such reactions are endoergic, but again there is wide variation, and in one case ($Y = CH_2PMe_2$, $Z = C_6F_5$) exoergic behaviour is found. There is a close linear relationship ($R^2 = 0.948$) between the activation and reaction free energies. The effect of PCM toluene is typically to reduce the activation barrier slightly (0.2 to 20 kJ $mol^{-1}$), but to markedly reduce the endoergic reaction energy (by up to 39 kJ $mol^{-1}$) by stabilisation of the more polar transition state and hydrogenated product relative to the less polar reactant complex.

*iv) Hydrogenation of achiral substrates*

Free energy profiles for hydrogenation of a set of simple, achiral substrates were then calculated, again using relaxed potential energy scans starting from intermolecular complex formed between hydrogenated catalyst and substrate. Several possible reaction coordinates were considered in each case: typically, scans of H…C distances from pre-reactive complex formed between hydrogenated catalyst and substrate were used. From these, possible starting points for transition state searches were extracted manually, and stationary points corresponding to transition states located, each of which was characterized as such *via* normal mode calculation and manual inspection of the normal mode corresponding to the imaginary eigenvalue. IRC profiles were used as the primary criteria of whether a TS so located

is relevant to the reaction of interest, and also whether reactions were concerted, synchronous or stepwise. Initial calculations were based around **2a** X = $CH_2$, Y = $CH_2NH_2$ and Z = $CH_3$ due to its small size, FLP character and typical value of energetics for hydrogen dissociation noted in Table 4.

With ethene as the substrate, reaction profile modelling proceeded smoothly, locating three stationary points on the PES, as shown in Figure 1. The transition state that links reactant with product involves motion of both hydrogen atoms from the catalyst to the substrate, indicating a concerted, synchronous reaction. The free energy barrier for this reaction in toluene is calculated to be 87.4 kJ $mol^{-1}$, and the overall free energy change -201.1 kJ $mol^{-1}$, indicating a highly exoergic process with a relatively low barrier, as required for a feasible hydrogenation catalyst. Repeating the process with Y = $CH_2PH_2$ results in similar synchronous profile with a free energy of activation = 42.8 kJ $mol^{-1}$ and overall free energy change of -278.2 kJ $mol^{-1}$. The reduced barrier on use of a phosphine base may be a result of the lower proton affinity of such centres, allowing this hydrogen to be lost to ethene more easily, although this must be balanced against the higher barrier for hydrogen dissociation noted above.

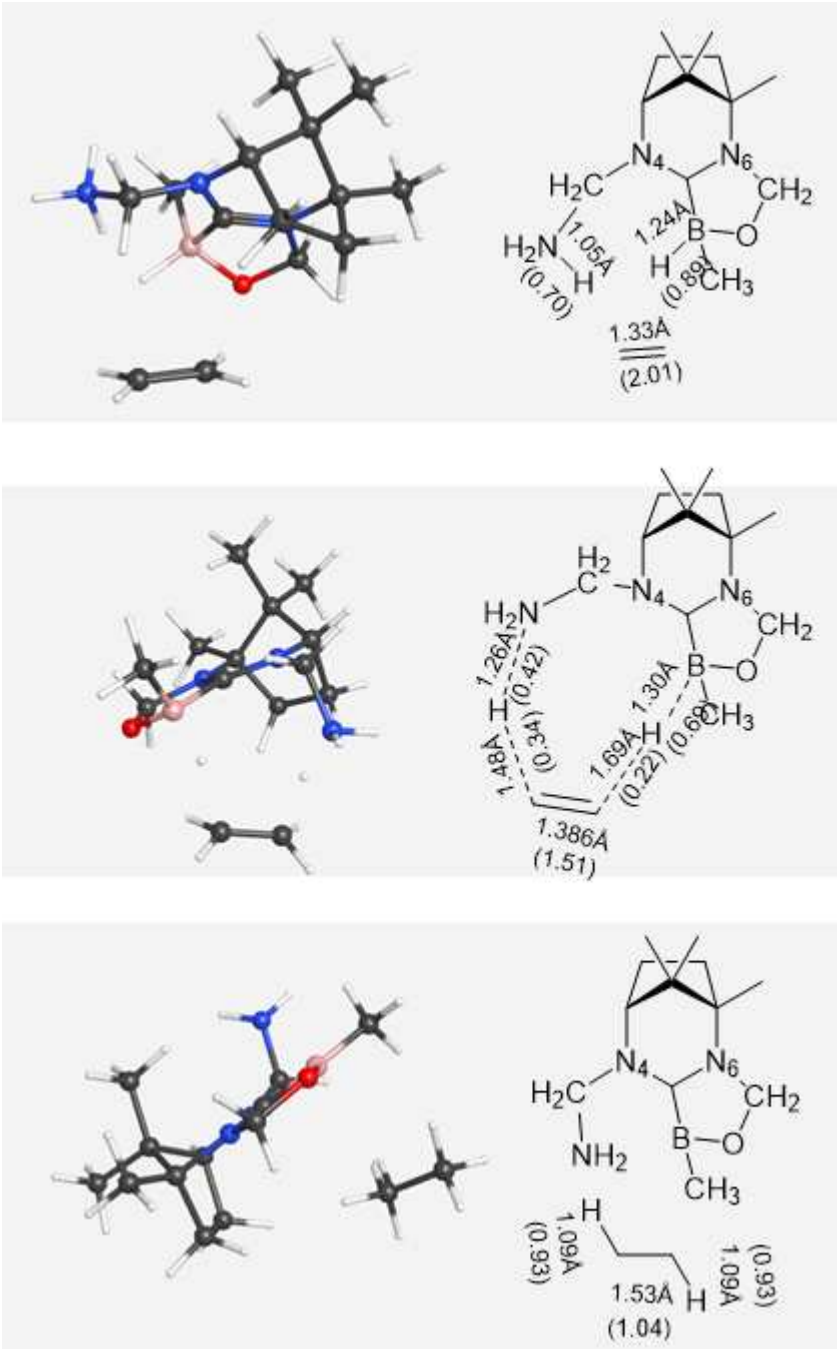


**Figure 1** Geometries of stationary points of PES for hydrogenation of ethene; top: reactant, middle: TS; bottom: product. Also shown are selected bond lengths and Wiberg bond orders (in parenthesis).

Figure 1 provides further evidence for the synchronous nature of ethene hydrogenation, showing that bond lengths and orders of both incipient C—H bonds change between reactant and TS. Details suggest that the TS is “early”, as evidenced by C—H bond orders of 0.2-0.3, and also somewhat asymmetrical in that hydrogen from N—H is transferred slightly more

than that from B—H at this point on the PES. The C—C bond order of 1.5 is consistent with a synchronous reaction.

The same procedure was then applied, with the same catalysts, to the hydrogenation of formaldehyde. The reactant complex with this more polar substrate contains close O…H—N and C…H—B contacts. Following relaxed potential energy scans of C…H and B…H distances, a transition state was located corresponding to movement of hydrogens, with a free energy barrier in toluene of 32.2 kJ mol$^{-1}$. IRC showed that this connects the reactant and "product" *via* a concerted, synchronous reaction. The "product" corresponds to the expected methanol molecule, but in close association with the now free borenium Lewis base, corresponding to an overall free energy change of -139.2 kJ mol$^{-1}$. A further barrier of 20.0 kJ mol$^{-1}$ is required to liberate methanol from the regenerated catalyst, an endoergic process leading to an overall energy change from reactants to products of -114.5 kJ mol$^{-1}$. Figure 2 confirms the synchronous nature of the reaction with formaldehyde, both N—H and B—H bonds significantly lengthened and weakened by first TS, and also that this is again "early" with C—H bond orders of less than 0.2.


**Figure 2** Comparison of change in bond lengths (bond orders) of the key bonds participating in hydrogenation of formaldehyde

Carrying out the same process for acetone yields a similar profile, in which a TS corresponding to synchronous movement of both hydrogens links reactant and product, the latter again being in a close association of alcohol with borenium Lewis acid. The free energy barrier for this process is 45.5 kJ mol$^{-1}$, *i.e.* slightly higher than for formaldehyde, and the reaction is

exoergic by -130.5 kJ mol$^{-1}$. As with formaldehyde, a second barrier for release of free product (propan-2-ol) from the catalyst must be overcome: in this case, this is actually higher than the barrier for hydrogenation at 81.3 kJ mol$^{-1}$. Product release is endoergic, such that the overall energy change to yield free catalyst plus product is -51.9 kJ mol$^{-1}$. Figure 3 shows a concerted but asynchronous pathway for hydrogenation, with a markedly greater bond order for transfer from N—H to C than that for B—H. This is notably dissimilar to that for formaldehyde, and may have its origin in the greater steric bulk of the ketone over the simple aldehyde.

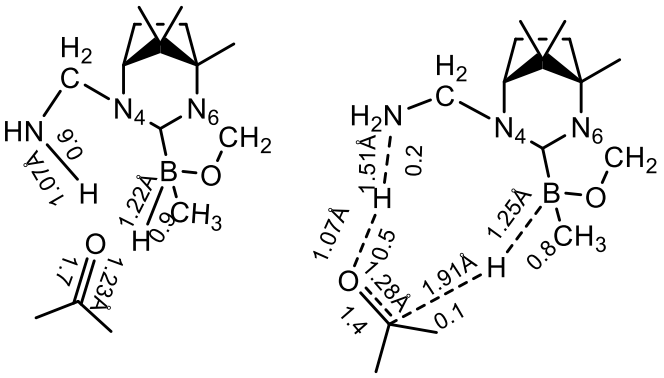


**Figure 3** Comparison of change in bond lengths (bond orders) of the key bonds participating in hydrogenation of acetone

*v) Hydrogenation of prochiral substrate*

A more challenging task is to examine the preferential hydrogenation of different faces of prochiral substrates, using acetophenone as an example. A total of 10 pre-reactive complexes of this substrate in intermolecular contact with the hydrogenated catalyst were optimised and characterised as true minima. Of these, six had the catalyst on the *Re*- face of the substrate, and four on the *Si*- face. The lowest energy conformation of each was initially selected to map out energy profiles through relaxed potential energy scans in simulated toluene, although dependence on starting position will be considered below. Following the results obtained for formaldehyde and acetone, we find a concerted pathway for hydrogenation of each face, confirmed by IRC calculation to link reactant complex and product of alcohol bound to borenium through close B…O contact. Attack on the *Si*- face has a free energy barrier of 32.62 kJ mol$^{-1}$ and an overall free energy change of -140.05 kJ mol$^{-1}$, while attack at the *Re*-face has a free energy barrier of 38.84 kJ mol$^{-1}$ and overall change of -142.38 kJ mol$^{-1}$. The relative energies of hydrogenation on both faces is summarised in Figure

4. Using a simple Arrhenius model for reaction rate and assuming the pre-exponential factor for *Re*- and *Si*- is identical, this corresponds to a relative rate for *Si*- attack over *Re*- attack of 15.5 at 273 K. This suggests that such an inherently chiral, intramolecular FLP has the correct design features to act as an enantio-selective hydrogenation catalyst. However, it does not yet compete with the best reported chiral FLP hydrogenation catalysts:[23] we hope to use the results obtained here to design more selective systems.

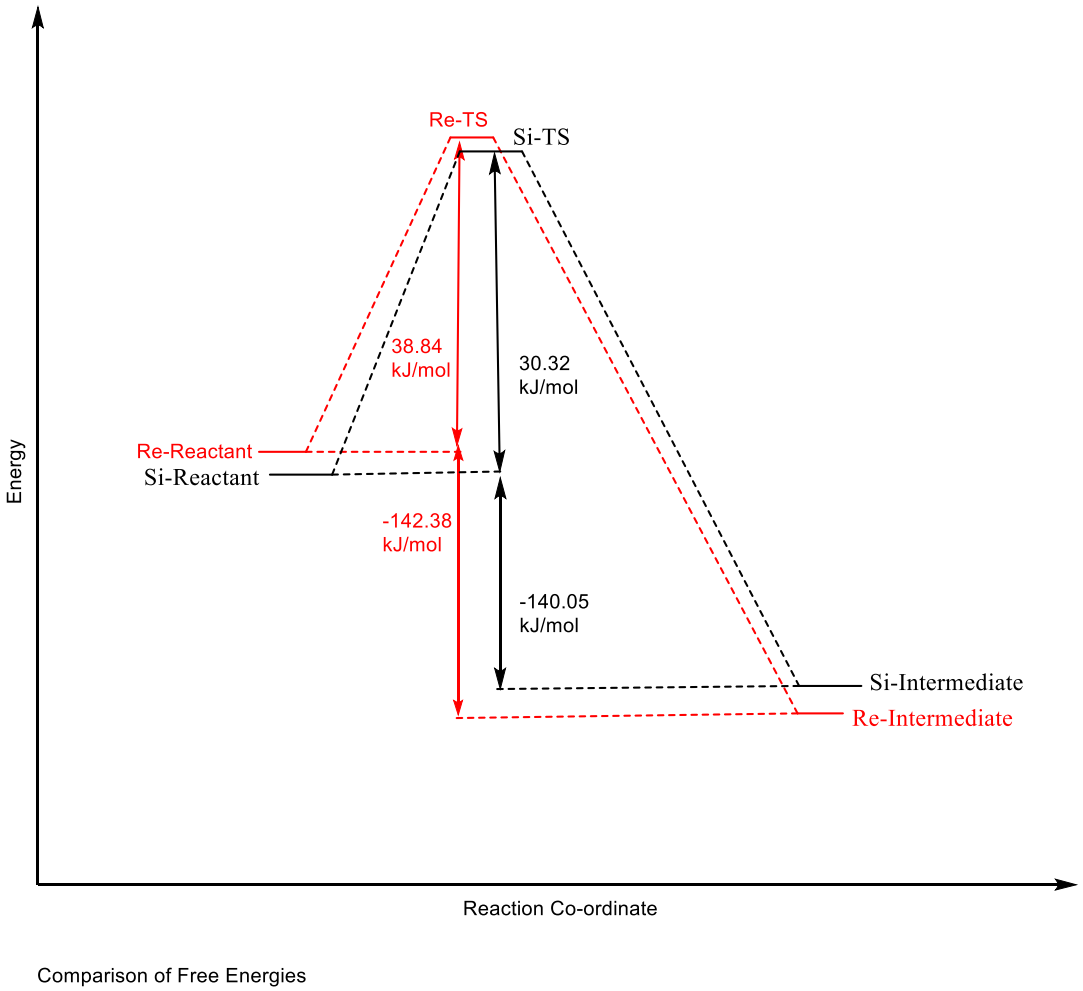


**Figure 4** Comparison of free energy for attack of FLP on Re- and Si-face of acetophenone.

The reactive complexes obtained as a result of IRC calculations from *Re*- and *Si*- transition states are almost identical to those used as starting points: the energy difference is less than 0.2 kJ $mol^{-1}$ from that used as the start point for potential energy scan. Moreover, transition states obtained from alternative starting points than the lowest energy one are identical to those discussed above, and after IRC calculation return to the same reactive complex. We are therefore confident that results obtained are not strongly dependent on starting point, and

hence that a more thorough coverage of the conformational space of reactive complexes is not required in order to obtain reliable free energy profiles. In this context, use of relaxed scans seems valuable: for both faces, a single reaction coordinate of H…C distance corresponding to hydride attack was sufficient to generate suitable starting points for subsequent TS searches. This, coupled with the flat intermolecular PES, allows adjustment of substrate-catalyst orientation.

Bond lengths and orders (Figure 5) indicate a concerted but asynchronous reaction mechanism similar to that for acetone. Proton transfer from N—H to O is notably further advanced than hydride transfer from B—H to C, with a bond order of 0.4 in the former, compared to just 0.1 in the latter. This may be due to the increased steric bulk or decreased nucleophilicity of the carbonyl C of the ketone substrate relative to aldehydes or smaller ketones. It is also notable that hydrogenation of both *Re*- and *Si*- faces exhibit identical bond lengths and orders, such that the difference in energy noted must have its origin elsewhere.

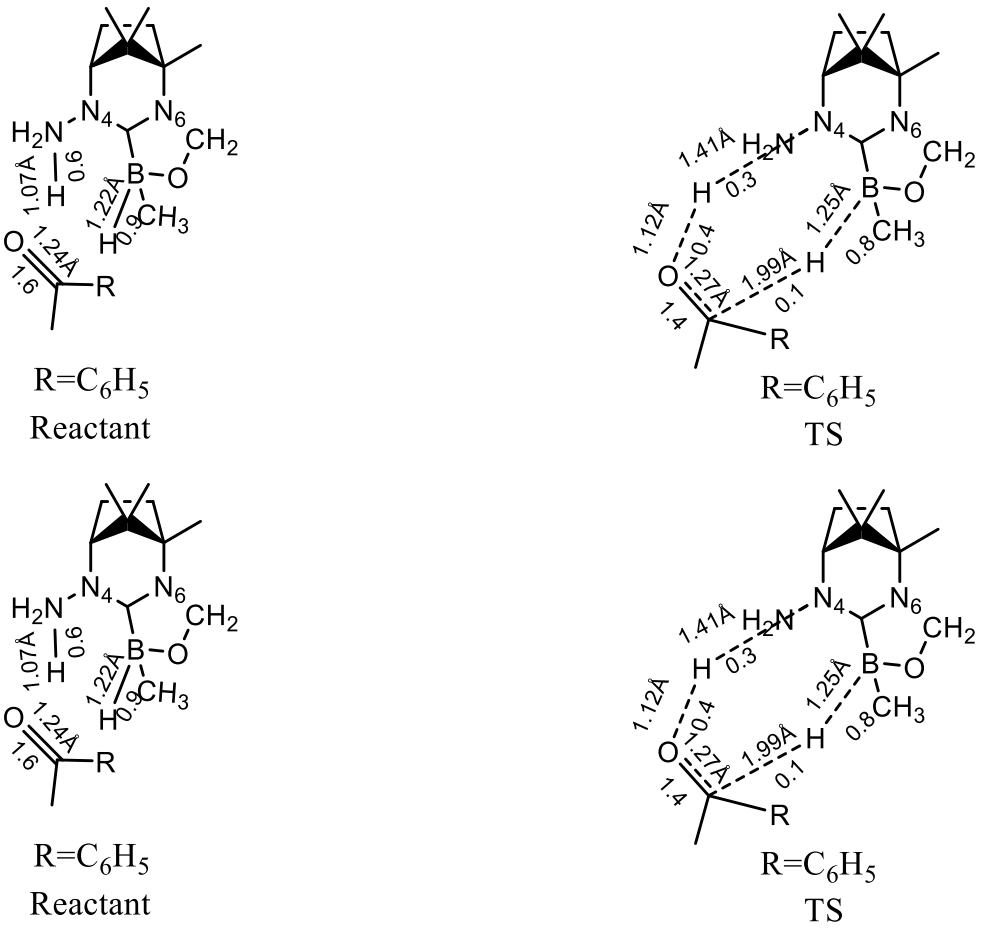


**Figure 5** Bond lengths (bond orders) of some key bonds participating in hydrogenation of acetophenone (top: *Si*-face, bottom: *Re*-face)

To explore the origin of the observed preference for attack at the *Si*- face, non-covalent interactions at each transition state were examined *via* QTAIM and NCIPlot analysis (Figure 6). QTAIM locates three bond critical points (bcp) corresponding to C—H…π interactions and a single C—H…O bcp in the *Si*- transition state, each representing catalyst-substrate interaction. In contrast, the *Re*- TS contains bcp's for two C—H…H—C contacts and one C—H…O bcp. The electron density at the bcp is between 0.005 and 0.010 au for all such contacts. NCIPlot indicates differences between transition states, most notably in the interactions of the aromatic ring of the substrate. Taken together, QTAIM and NCIPlot analyses suggest that the subtle balance of weak non-covalent interactions introduced by the asymmetry built into the catalyst is responsible for the observed difference in barrier. In particular the interactions between the aromatic moiety of the substrate differ markedly between the transition states located.

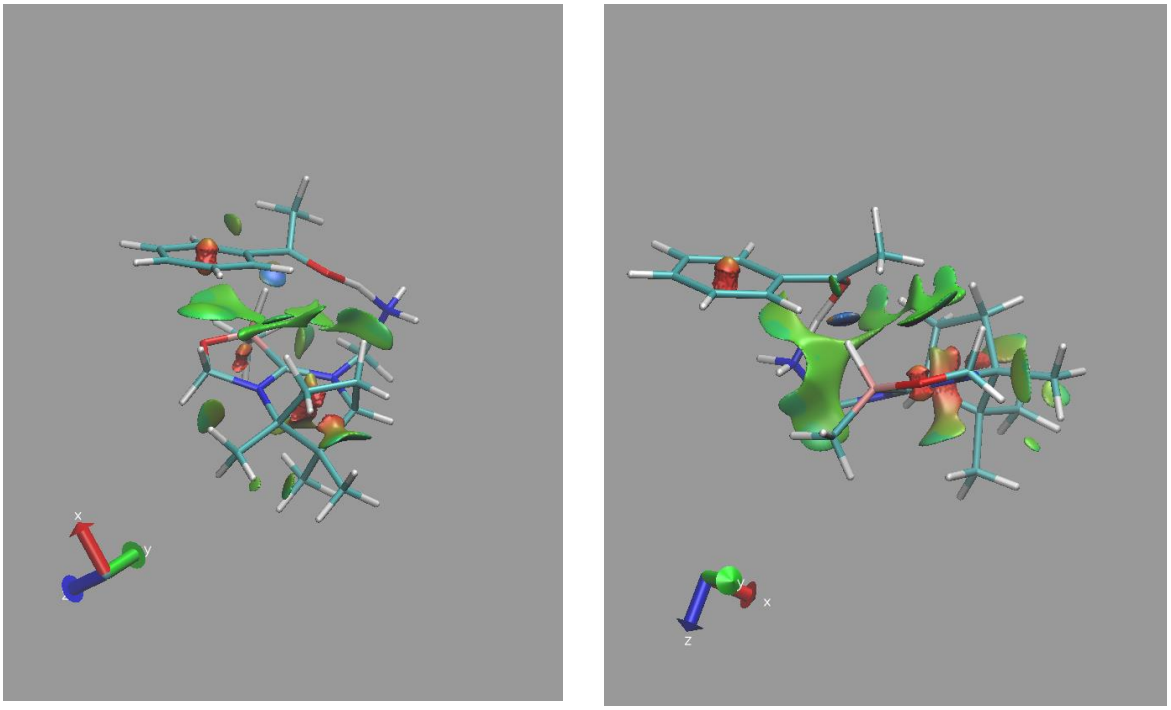

**Figure 6** NCIPlot for (left) *Si*- and (right) *Re*- transition states, plotted as isosurface of reduced density gradient. Green indicates weakly attractive interactions

**Conclusions**

We have used DFT to explore the potential for chiral intramolecular hydrogenation catalysts based on frustrated Lewis pair chemistry. The general design employs a chiral carbene derived from camphor bound to a Lewis acidic borenium centre, with linkers designed to place a Lewis base in proximity to the acidic centre without being able to form a conventional adduct. We find that amine and phosphine Lewis bases with $CH_2$ or phenyl linkers exhibit FLP character, whereas $CH_2CH_2$ linkers form adducts, as measured by Wiberg bond orders. Selected FLP systems are predicted to dissociate $H_2$, the barrier to which can be tuned by suitable choice of Lewis base and substituent on B between values as small as 35 and as high as 184 kJ $mol^{-1}$. Hydrogen dissociation is typically endoergic, but a combination of tertiary phosphine base and $C_6F_5$ on B is predicted to yield exoergic character. Weak bases such as furan and thiophene are found to be unable to split $H_2$.

Having dissociated $H_2$, which involves addition of a proton to Lewis base and hydride to Lewis acid, the catalysts' ability to hydrogenation some model substrates was examined.

Hydrogenation of ethene is found to proceed through a concerted, synchronous mechanism with rather low barriers. A similar mechanism is found for carbonyl substrates: formaldehyde is very similar to ethene, while the extra bulk of acetone leads to a less symmetric and synchronous mechanism. In both of these cases, the product alcohol is found to bind tightly to the borenium centre, thus requiring further input of energy to release the product and regenerated catalyst. Examination of a prochiral substrate, acetophenone, suggests that the proposed scaffold has some promise as an enantioselective catalyst: we predict that hydrogenation at the *Si* face should have a small but significant preference over the *Re* face. Simple transition state theory arguments suggests kinetic preference for attack at *Si* of around 15:1, ascribed to favourable C—H…π interactions in the relevant TS. Attempts to synthesise and test catalysts based around these designs are ongoing, and we hope to report the results of this in a future publication.

**Acknowledgements**

We are grateful to Advanced Research Computing @ Cardiff (ARCCA) and Supercomputing Wales for provision of computing resources.

**References**


[1] See D. W. Stephan, *Science*, 2016, **354**, aaf7229 and references cited therein.

[2] H. Brown, H. Schlesinger, S. Cardon, *J Amer. Chem. Soc.*, 1942, **64**, 325-329.

[3] a) J. McCahill, G. Welch. D. Stephan, *Angew. Chem. Int. Ed.*, 2007, **46**, 4968-4971; b) G. Welch, R. Juan, J. Masuda, D. Stephan, *Science*, 2006, **314**, 1124-1126. C) G. Welch and D. Stephan, *J. Amer. Chem. Soc.*, 2007, **129**, 1880-1881.

[4] a) M. Oestreich, J. Hermeke, J. Mohr, *Chem. Soc. Rev*, 2015, **44**, 2202-2220; b) D. Scott, M. Fuchter A. Ashley, *Chem. Soc. Rev*, 2017, **46**, 5689-5700.

[5] W. Meng, X. Feng, H. Du, *Acc. Chem. Res.*, 2018, **51**, 191−201.

[6] D. Holschumacher, T. Bannenberg, C. G. Hrib, P. G. Jones, M. Tamm, *Angew. Chem*. 2008, **120**, 7538 –7542.

[7] a) M. Pu, T. Privalov, Isr. J. Chem. 2015, 55, 179 – 195; b) Green Energy Environ., 2019, **4**, 20-28.

[8] J. Lam, B. Guenther, J. Farrell, P. Eisenberger, B. Bestvater, P. D. Newman, R. L. Melen, C. Crudden, D. W. Stephan, *Dalton Trans* 2016, **45**, 15303-15316.

[9] a) J. Clarke, P. Eisenberger, S. Piotrkowski and C. Crudden, *Dalton Trans.*, 2018, **47**, 1791-1795. b) L. Wang, S. Dong, C. Daniliuc, L. Liu, S. Grimme, R. Knitsch, H. Eckert, M. Hansen, G. Kehr and G. Erker, *Chem. Sci.*, 2018, **9**, 1544-1550. c) J. Légaré Lavergne, A. Jayaraman, L. Misal Castro, É. Rochette and F. Fontaine, *J. Amer. Chem. Soc*., 2017, **139**, 14714-14723. d) Z. Dong, Z. Li, X. Liu, C. Yan, N. Wei, M. Kira and T. Müller, *Chem. Asian J.*, 2017, **12**, 1204-1207. e) K. Chernichenko, B. Kótai, M. Nieger, S. Heikkinen, I. Pápai and T. Repo, *Dalton Trans.*, 2017, **46**, 2263-2269.

[10] a) L. Hounjet, C. Bannwarth, C. Garon, C. Caputo, S. Grimme and D. Stephan, *Angew. Chem*., 2013, **125**, 7640-7643. b) L. Greb, P. Oña-Burgos, B. Schirmer, S. Grimme, D. W. Stephan, J. Paradies, *Angew. Chem.*, 2012, **124**, 10311-10315.

[11] a) I. Peuser, R. Neu, X. Zhao, M. Ulrich, B. Schirmer, J. Tannert, G. Kehr, R. Fröhlich, S. Grimme, G. Erker D. W. Stephan, *Chem. Eur. J.*, 2011, **17**, 9640-9650. b) F. Fontaine and É. Rochette, *Acc. Chem. Res.*, 2018, **51**, 454-464.

[12] É. Rochette, H. Boutin, F. Fontaine, *Organometallics*, 2017, **36**, 2870-2876.

[13] C. Tang, Q. Liang, A. Jupp, T. Johnstone, R. Neu, D. Song, S. Grimme, D. W Stephan, *Angew. Chem. Int. Ed.*, 2017, **56**, 16588-16592.

[14] Y. Zhao and D. G. Truhlar *Theor. Chem. Acc.* **2008**, *120*, 215–241.

[15] (a) R. Ditchfield, W. J. Hehre, J. A. Pople, *J. Chem. Phys.* 1971, 54, 724–728. (b) P. C. Hariharan and J. A. Pople, *Theor. Chim. Acta* 1973, **28**, 213–222.

[16] M. J. Frisch, et al. *Gaussian09*; Gaussian Inc.: Wallingford, CT, 2009.

[17] J. Tomasi, B. Mennucci, R. Cammi, *Chem. Rev.* **2005**, *105* (8), 2999–3094.

[18] A. E. Reed, L. A. Curtiss, F. Weinhold, *Chem. Rev.* **1988**, *88* (6), 899–926.

[19] R. F. W. Bader, *Atoms in Molecules: A Quantum Theory* Clarendon, Oxford 1994.

[20] T. A. Keith, *AIMAll*; TK Gristmill Software: Overland Park KS, USA, 2017.

[21] J. Contreras-García, E. R. Johnson, S. Keinan, R. Chaudret, J.-P. Piquemal, D. N. Beratan, W. Yang, *J. Chem. Theor. Comput.* **2011**, *7*, 625–632.

[22] H. Böhrer, N. Trapp, D. Himmel, M. Schleep, I. Krossing *Dalton Trans.* **2015**, *44*, 7489–7499.

[23] J. Lam, S. Sampaolesi, J. H. W. LaFortune, J. W. Coe, D. W. Stephan *Dalton Trans*., 2019, **48**, 133-141.